Photoionization of helium, neon and argon in the 60-230 eV photon energy range

J. Phys. B: Atom. Molec. Phys., Vol. 5, December 1972. Printed in Great Britain.

Photoionization of helium, neon and argon in the 60–230 eV photon energy range

W S WATSON

Department of Natural Philosophy, The University, Glasgow, W2

MS received 2 June 1972

Abstract. The photoionization absorption coefficients of helium, neon and argon have been measured by single beam photometry in the 60–230 eV photon energy range using a synchrotron radiation source and channel electron multiplier photodetection. The accuracy of most of the data is $\pm 3\%$ rising to $\pm 5\%$ for a few cases in helium. Agreement with theory is typically better than 20% for photon energies up to 150 eV with greater discrepancies at higher energies especially for helium and argon.

1. Introduction

Accurate atomic wavefunctions are a prerequisite of any calculation investigating the properties of the isolated atom (eg energy levels), or atomic interactions (eg electron–atom collisions). Comparison of theory and experiment for the photoionization process provides a sensitive test of wavefunction accuracy and it is for this reason that the photoionization data available for helium, neon and argon have been improved and extended in the present work. Rare gas species were chosen as they are monatomic at room temperature and provide a good approximation to the isolated atom case considered by theory.

Photoionization studies of the above gases involve the techniques of vacuum ultraviolet spectroscopy since the rare gases have high ionization potentials resulting from their closed subshell configuration, for example 24·56 eV for helium. Until recently, a large photon energy gap existed in the available data due to the non-availability of an intense radiation source between soft x ray sources ($h\nu > 230$ eV) and emission line sources ($h\nu < 60$ eV). This is an important region where cancellation in the electric dipole matrix element which governs the spectral variation of the photoionization absorption coefficient, makes the theoretical calculations particularly sensitive to choice of wavefunctions. In the last few years, synchrotron radiation emitted by electron synchrotrons has provided a powerful continuum of electromagnetic radiation in this spectral region.

In the present experiment, the radiation emitted by the 340 MeV Glasgow Electron Synchrotron has been used to study the variation of the photoionization absorption coefficients of helium, neon and argon in the 60–230 eV photon energy range.

2. Experimental method

2.1. Introduction

Neglecting the limited regions of the spectrum where autoionization is possible, photoionization is the only available attenuation process in monatomic gases for photons with sufficient energy to ionize the atomic species, (Samson 1964a, Matsunaga *et al* 1965) but not greater than 1 KeV beyond which Thomson scattering and ultimately Compton scattering become important. Therefore, the photoionization absorption coefficient, k, of a monatomic gas for a photon energy, $h\nu$, in the above range is given by the Lambert–Beer law,

$$k = \left(\frac{p_o T}{p T_0 x}\right) \ln\left(\frac{I_0}{I}\right) \tag{1}$$

where I_0 and I are the radiation intensities for photons of energy $h\nu$ which are incident on and transmitted by x cm of gas at constant pressure, p Torr, and temperature, T K, while p_0 and T_0 are the normal pressure and temperature, that is $p_0 = 760$ Torr and $T_0 = 273$ K.

A preliminary investigation of the absorption spectra was made using high resolution and radiation detection by photographic emulsion (Watson and Morgan 1969). No strong discrete structure was observed in the spectra over the region proposed for the present investigation, therefore it was decided to measure k at fixed values of $h\nu$ with energy intervals ranging from 3 eV to 20 eV.

Single beam photometry was used to measure I_0 and I to a statistical accuracy of $\pm 1\,\%$ while single measurements of the gas parameters p, x and T were typically better than $\pm 2\,\%$ accurate. Therefore, ideally, repeated measurement of I_0, I, p, x and T should provide extremely accurate values of k.

2.2. Apparatus

As shown in figure 1 the single beam photometry (SBP) experimental set up can be split into three main elements, the synchrotron radiation source, the absorption cell and the spectral analyser–detector.

Synchrotron radiation emitted tangentially from the synchrotron electron orbit passed down a 6 cm OD stainless steel beam tube to be analysed by a 1 m grazing incidence spectrometer, with channel electron multiplier photodetection, positioned with its entrance slit 5 m from the source tangent point. The absorption cell, with length, $x = 0{\cdot}75 \pm 0{\cdot}005$ m defined by Zapon films (~ 2000 Å thick) was an integral part of the beam tube.

The three elements of the SBP system will now be considered in greater detail.

2.2.1. Synchrotron radiation source. The properties of synchrotron radiation have been well documented (Haensel and Kunz 1967, Sokolov and Ternov 1968, Godwin 1969). A continuum of highly directional, highly polarized electromagnetic radiation is emitted in the forward direction of the instantaneous velocity vector of the electrons which are accelerated in the synchrotron. For the 340 MeV Glasgow Electron Synchrotron this continuum has a maximum photon intensity at about 60 eV with this maximum moving to lower photon energies for lower accelerated electron energies. In the Glasgow machine, a bunch of approximately 3×10^9 electrons travelling in an orbit of 1·25 m

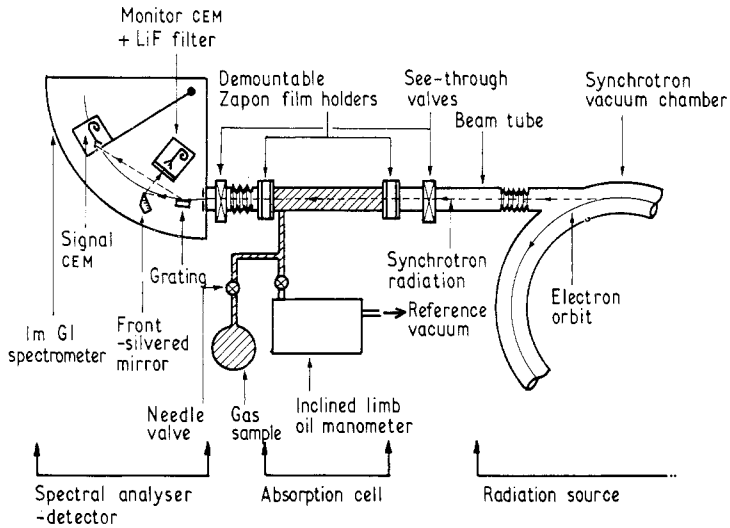

Figure 1. Schematic diagram of experimental set-up

radius with an orbit frequency of 38 MHz experiences a sinusoidal energy variation over a half cycle of 14×10^{-3} second duration, repeated four times a second. The maximum electron energy, E_{max}, can be varied in 10 MeV steps from 100 MeV to 340 MeV. The flux for photon energies of 60 eV into the 100 μm wide entrance slit of the spectrometer is calculated to be $8{\cdot}8 \times 10^{5}$ photons s^{-1} eV^{-1} for $E_{max} = 207$ MeV rising to $2{\cdot}8 \times 10^{7}$ photon s^{-1} eV^{-1} for $E_{max} = 340$ MeV. Comprehensive calculations of the expected flux have been performed for a large number of photon and machine energies. (Lang 1969, 1970, Lang 1972 private communication).

2.2.2. Absorption cell. Ideally, the absorption cell should be placed behind the exit slit of the analyser thus avoiding the possibility of a build up of photo-produced species which might have occurred in the present set-up where all the radiation to be analysed first passed through the cell. This arrangement was dicatated by the spectrometer design and in practice photoproduced contamination was not observed.

The Zapon films defining the ends of the cell covered vertically aligned slots ($1{\cdot}2 \times 0{\cdot}4$ cm) cut in demountable film holders thus allowing radiation transmitted by the films to be incident on the 1 cm long vertical entrance slit of the spectrometer. The films were strengthened by one-dimensional grids of 44 SWG wire with a grid spacing of 0·1 cm attached to the film holders with epoxy resin (Araldite).

It was decided not to use a gas flow system but simply to introduce the sample gas into the evacuated cell and then to isolate the cell allowing the gas to attain dynamic and thermal equilibrium. The advantages of this method, namely the uniform temperature and pressure of the gas in the cell have been experimentally proved to outweigh the possible disadvantages such as sample contamination by outgassed or photo-produced species. Grade X gases (British Oxygen Company) were used throughout the experiment. The helium and argon samples were 99·9995 % pure and the neon was 99·95 % pure.

The pressure of the gas was measured by an inclined-limb oil manometer specially designed by the author (details to be published). This device was capable of measuring

pressures $p \geqslant 0{\cdot}2$ Torr to $\pm 2\%$ or better and pressures in the range, $0{\cdot}1$ Torr $\leqslant p < 0{\cdot}2$ Torr to $\pm 5\%$ accuracy as proved by comparison with a factory calibrated diaphragm capacitor manometer (MKS Baratron Type 77). The pressures used in the experiment were in the $0{\cdot}1$ Torr $< p < 5$ Torr range.

2.2.3. Spectral analyser–detector. The 1 m. grazing incidence spectrometer used had a horizontal Rowland Circle and incorporated a platinized, 1152 lines mm^{-1}, Bausch and Lomb replica grating set an angle of incidence of $87{\cdot}5°$ resulting in a blaze wavelength of 40 Å ($h\nu = 310$ eV). The reciprocal linear dispersion was $0{\cdot}7$ Å mm^{-1} at 30 Å ($h\nu = 413$ eV) increasing to $2{\cdot}1$ Å mm^{-1} at 300 Å($h\nu = 41{\cdot}3$ eV). Therefore, as slit widths from 100 to 400 μm were used, the maximum bandwidth was 1 Å, with $0{\cdot}2$ Å being more typical.

Photodetection was by means of a channel electron multiplier (Mullard, type B419BL) mounted behind the exit slit of the spectrometer. In what follows this will be called the signal CEM. Synchrotron electron beam variations were normalized by a monitor CEM (Mullard, type X312BL) which responded only to electron beam variations and was independent of gas pressure p. This was achieved by allowing the monitor to respond to the radiation specularly reflected from the grating but which had passed through a lithium fluoride filter which cut out high energy radiation capable of being attenuated by the gas sample.

The CEMs were used in photon counting mode each being connected to a fast (~ 100 MHz) electronics channel comprizing a gain of 16 amplifier (EG and G, AN101), a discriminator/trigger (EG and G, TR104S) and a scalar (BORER, Type 613). The ratio of the signal CEM counts to a fixed number of monitor CEM counts, gives a measure of I, or I_0 if $p = 0$. In practice the counting cycle was automatically stopped after 10^4 monitor counts while the bandwidth was adjusted to make the signal and monitor count rates approximately equal at around 300 counts s^{-1}. Therefore, $\pm 1{\cdot}4\%$ statistical accuracy (66% confidence) on the ratio was usually obtained in less than one minute. In general the count rate was limited not by lack of radiation intensity but by the gain degradation of the CEMs with increased count rate. Careful attention was paid to the maximum allowable count rate used and also to the setting of pulse height discrimination levels thus eliminating any error from this cause.

2.3. Data collection and analysis

The photoionization coefficient k for each photon energy considered was obtained by measuring I_0 and I for several values of pressure p and then plotting $\ln(I_0/I)$ against p yielding in theory a straight line graph of gradient $(T_0 x/p_0 T)k$ and hence giving k. A typical point on such a graph was produced by the following procedure. Two values of I_0, each of approximately $\pm 1{\cdot}4\%$ statistical accuracy were taken with $p = 0$, gas was then introduced into the absorption cell and allowed to settle for 1–2 minutes, four values of I were then obtained during which time the pressure p was measured at least twice to test its stability, finally the cell was evacuated and a further two values of I_0 taken. Preliminary data indicated that such plots were in general not linear but curved due to the contamination of the first order diffracted spectrum by higher order spectra. If only second order radiation is present the Lambert–Beer Law is modified to give:

$$\ln\left(\frac{I_0}{I}\right) = k_1\left(\frac{T_0 x}{p_0 T}\right)p + \ln\left(\frac{(1+\alpha)}{1+\alpha\exp\{(k_1-k_2)(T_0 x/p_0 T)p\}}\right) \tag{2}$$

where I_0 is the total incident intensity detected, I is the total transmitted intensity detected, k_1 and k_2 are the photoionization coefficients for first and second order radiation respectively and α is the ratio of the intensity of the second order radiation detected to the first order radiation intensity detected at a given first order wavelength position. The method adopted in the present experiment was to keep α as small as possible and so reduce the correction term on the RHS of expression 2; this can be done by using as small values of E_{max} as are experimentally possible, since, to a first approximation, α varies as a positive power of E_{max}. When this was done, log plots taken for values of E_{max} differing by tens of MeV were linear to within experimental error for ratios $I_0/I \leqslant 20$, but the plots had slightly different gradients varying systematically with E_{max} as shown in figure 2. Simplifying expression 2 using the conditions that $\alpha \ll 1$

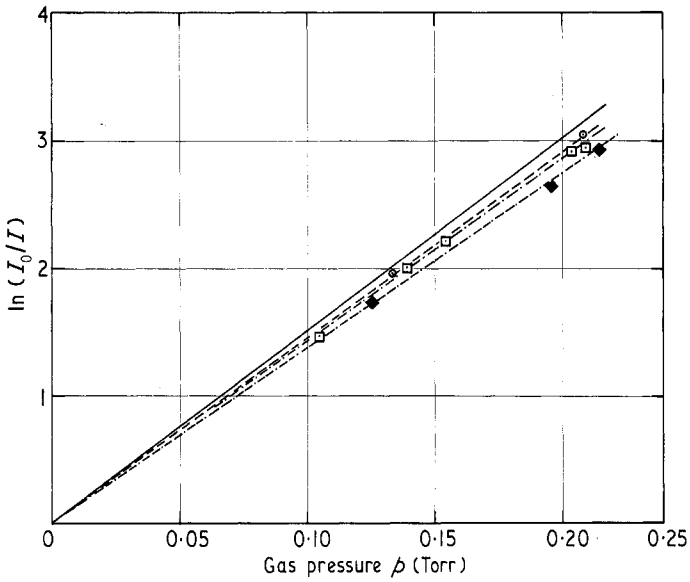

Figure 2. Log plot for neon photoabsorption at $h\nu = 66{\cdot}9$ eV for different synchrotron electron energies. – – ⊙ – – $E_{max} = 216$ MeV; – · – ⊡ – · – $E_{max} = 230$ MeV; · – – ◆ – – · $E_{max} = 242$ MeV; ——— calculated log plot for zero 2nd order radiation contribution.

and that the correction term is linear in p, yields the following:

$$k_a = k_1 - \alpha(k_1 - k_2)$$

where k_a is the apparent photoionization coefficient obtained from the gradient of a log plot for some maximum machine energy, E_{max}. Therefore, k_1 could be found by obtaining a least squares fit to expression (3) knowing k_a and the corresponding α values. In practice the α values were not known absolutely as they depend on grating and detector efficiencies and also on the photon energy sensitive transmission of the Zapon films. However, for a given photon energy and machine energy, α is proportional to the calculable ratio of second order radiation to first order radiation emitted by the synchrotron and so k_1 could still be obtained by this method. It should be noted that k_a values were obtained from log plots containing a minimum of three points including the origin, and

were known to a typical accuracy of $\pm 1\%$. The corrected value k_1 seldom differed from the lowest corresponding k_a value by more than 10% and was never greater than 4% above the highest corresponding k_a value. The accuracy of the correction procedure was such that for a given photon energy, the corrected k_1 values obtained from sets of data each with different α values, due to the use of different Zapon films, were, on average, 3% different. In this way values of k_1 were obtained for the lower photon energies used in the experiment. At higher photon energies α tends to zero and so the correction becomes negligible but the first order spectrum becomes contaminated instead by radiation scattered by the grating. As the percentage of stray radiation is a function of machine energy the true coefficients k could be extracted from the experimental data by a similar procedure and to the same accuracy as for the second order contamination case.

Using these processes of data reduction the photoionization coefficients of helium, neon and argon were obtained to an accuracy of $\pm 3\%$ for all cases except several high photon energy values in helium where the error rises to $\pm 5\%$ because of the very small values of the coefficient.

3. Results

3.1. Helium

The variation of the photoionization coefficient with incident photon energy is shown in table 1. In order to compare the results with theory, which generally considers only the $1s^2\ ^1S_0 \rightarrow 1s\epsilon p\ ^1P_1$ photoionization channel, corrections have been made to eliminate the contributions from simultaneous photoionization and photoexcitation, that is $1s^2\ ^1S_0 \rightarrow ns\epsilon p$ or $np\epsilon s (2 \leqslant n < \infty)$ and also double photoionization, that is

$$1s^2\ ^1S_0 \rightarrow \epsilon s\epsilon p.$$

Table 1. Helium photoionization coefficients

Photon energy (eV)	k (total) (cm^{-1})	$k(1s^2\ ^1S_0 \rightarrow 1s\epsilon p\ ^1P_1)$ (cm^{-1})
66·8	29·8	28·2
70·7	25·4	23·9
74·9	22·4	21·1
79·3	18·8	17·5
84·3	16·5	15·4
95·5	11·9	11·1
108·6	8·45	7·76
124·5	6·09	5·60
143·6	4·12	3·78
154·9	3·26	2·98
167·0	2·44	2·23
196·3	1·54	1·40
233·5	0·87	0·79

Error: $\pm 3\%$ for $h\nu \leqslant 154{\cdot}9$ eV
$\pm 5\%$ for $h\nu > 154{\cdot}9$ eV

The theoretical estimates of Brown (1970) for simultaneous photoionization and photoexcitation and of Byron and Joachain (1967) for double photoionization have been used to evaluate the required correction which ranges from 6% at 66 eV to 13% at 520 eV. Photoelectron studies by Samson (1969) and ion charge determinations by Carlson (1967) suggest a maximum uncertainty of 15% in this correction resulting in a 2% maximum uncertainty in the corrected values of k.

Figure 3 shows the present state of theory and experiment for $h\nu \geqslant 50$ eV, with the corrected experimental results and several theoretical estimates weighted by the factor

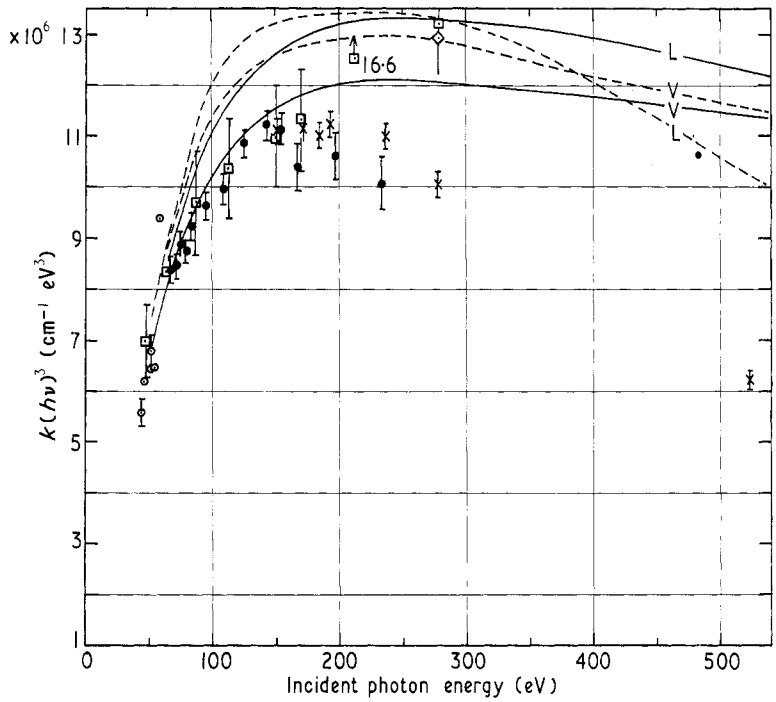

Figure 3. Photoionization coefficient of helium in the 50–550 eV photon energy range. Theory: ——— Bell and Kingston (1967, Hartree–Fock Ψ_{final}); — — — Bell and Kingston (1970, polarized orbital Ψ_{final}). Experiment: ⊡ Lukirskii *et al* (1964); ◇ Dershem and Schein (1931); ⊙ Samson (1964b); × Denne (1970); ● Present data.

$(h\nu)^3$ for ease of illustration. The consistency of the more recent experimental investigations is good as evidenced by the agreement of the present results with the lower photon energy double ion chamber work of Samson (1964b) and the soft x ray study of Denne (1970) using proportional counter detection. The results of Lowry *et al* (1965) using photographic detection down to $h\nu = 155$ eV have not been shown because of the large scatter of data in the higher photon energy range. However, the soft x ray results of Lukirskii *et al* (1964), which are normalized to those of Lowry *et al* because of gas purity uncertainties, are included because of the large photon energy range covered. These are compatible with later results except for $h\nu > 200$ eV where the small absorption coefficient of helium demands a high degree of gas purity to yield accurate information. The isolated determination of the coefficient at 278 eV by Dershem and Schein (1931) using photographic detection is 30% higher than the later studies although the error

quoted is 1%. It must be assumed that here again impurities in the helium sample affected the experimental accuracy.

The most comprehensive theoretical estimates are those of Bell and Kingston (1967, 1970) forming a natural extension to the work of Stewart and Webb (1963) whose dipole length and velocity results, using a 6-parameter Hylleraas initial state wavefunction and a Hartree–Fock final state wavefunction, agree well with Samson's data from threshold to $h\nu = 60$ eV. In addition to confirming the calculations of Stewart and Webb, Bell and Kingston have taken more account of electron correlation with more sophisticated initial states and polarized orbital continuum states which allow for the effect of the outgoing electron on the bound 1s electron. Length and velocity formulations with a 50-parameter initial function and both polarized orbital and Hartree–Fock continuum functions are illustrated in figure 3.

Comparison of theory and experiment indicates that for $h\nu < 160$ eV, the dipole velocity results with a Hartree–Fock continuum function are the best theoretical estimate with the other theoretical results being up to 20% high. For $h\nu > 160$ eV, the discrepancy between theory and experiment becomes very marked with the observed coefficients decreasing much more rapidly than predicted. It is unlikely that the higher photon energy experimental results are inaccurate by a factor capable of accounting for this disagreement as the most probable systematic error, namely sample gas impurity, would tend to bring theory and experiment into better agreement. Therefore the fault must lie with the theoretical estimates indicating the desirability of even better continuum representations and possibly the use of the dipole acceleration formulation at these higher energies.

This present study of theory and experiment aptly underlines the advantage of studying the variation of the photoionization coefficient at photon energies where cancellation in the dipole matrix element magnifies wavefunction discrepancies. At threshold in helium, theoretical coefficient values deduced from early, fairly crude models (eg Wheeler 1933) differ by 3% at most from highly sophisticated methods, whereas for $h\nu > 100$ eV, differences of 40% between recent estimates are not unusual.

3.2. Neon

The results for neon are shown in table 2. In this case no correction for multi-electron excitation channels has been made. Figure 4 shows the present data together with previous theory and experiment for $h\nu \geqslant 50$ eV; the results being weighted by the factor $h\nu^{2.5}$ since k is approximately proportional to $h\nu^{-2.5}$ for $h\nu > 180$ eV. Again excellent agreement is obtained with Samson's lower energy results (Samson 1965); however, the discrepancy of up to 16% with respect to Denne's results is worrying while the $\pm 7\%$ uncertainty in the values obtained by Haensel *et al* (1970) does not allow for an assessment of the source of the disagreement. The semi-empirical estimates of Henke *et al* (1957) are shown together with the isolated measurement of Dershem and Schein (1931) at $h\nu = 278$ eV.

The spectral variation of photoionization coefficient computed from three different theoretical models is also shown. McGuire (1968) adopts the unrelaxed core method, where the same potential is used in the calculation of the initial and final wavefunctions. Sewell (1965) accounts for a change in potential by assuming that the continuum state can be represented by a core of Ne^+ orbitals plus a free electron moving in the field of the ion. Amusya *et al* (1971) explicitly introduce multi-electron correlation in their random phase approximation calculations. These represent the most realistic coefficient

Table 2. Neon photoionization coefficients

Photon energy (eV)	k (total) (cm^{-1})
63·1	171·9
66·8	167·4
70·7	157·4
74·9	150·2
79·3	142·8
84·3	131·3
95·5	113.3
101·7	96·5
108·6	91·2
116·3	79·1
143·5	51·8
154·9	45·0
166·9	38·2
180·8	31·5
196·2	26·0
213·6	21·4
233·2	17·8

Error: ±3%

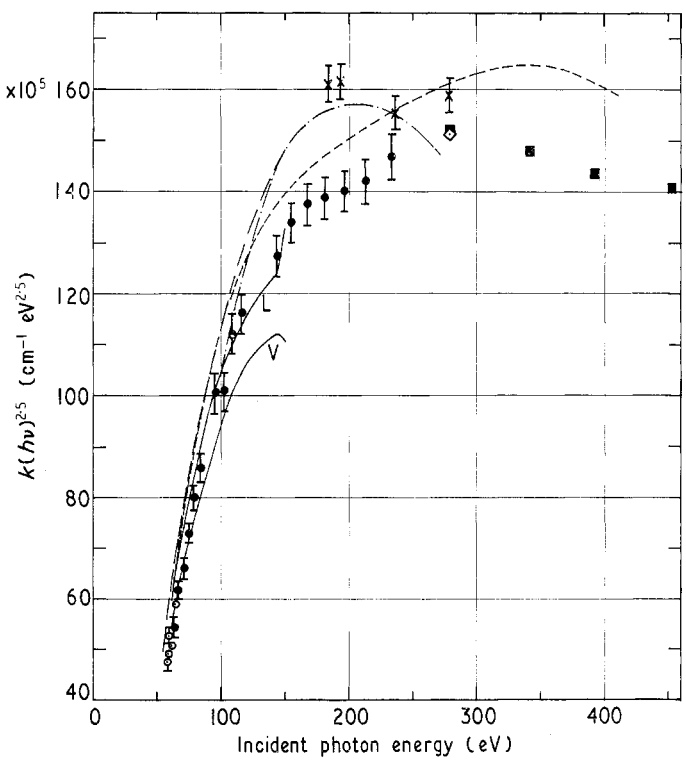

Figure 4. Photoionization coefficient of neon in the 50–450 eV photon energy range. Theory: ——— Sewell (1965, dipole length and velocity formulations); – – – McGuire, (1968); — — Amusya *et al* (1971). Experiment: ◇ Dershem and Schein (1931); ■ Henke *et al* (1957); ⊙ Samson (1965); × Denne (1970); – · – · – Haensel *et al* (1970) (±7% uncertainty); ● Present data.

calculations to date as evidenced by very good agreement with experiment for all rare gases.

Unfortunately, only the work of McGuire covers the total photon energy range of the present experimental results. In this range, the spectral variation of photoionization coefficient is predicted to within 10% while comparable agreement is obtained with the results of Samson at lower photon energies. This represents excellent agreement; however, the general adequacy of this model is made more dubious by its failure to predict accurately the threshold behaviour of heavier rare gases.

The other models previously mentioned are also in good quantitative agreement with experiment over their more limited photon energy ranges with an extension of the promising random phase approximation data being desirable.

3.3. Argon

Table 3 contains the results obtained for argon. As in neon, no correction is made for multi-electron excitation. Figure 5 shows the excellent agreement between recent experimental investigations, particularly the results of Samson (1964c), Denne (1970) and the present study. The maximum in the spectral variation of the photoionization coefficient is due to the nodal nature of the 3p electron wavefunction which causes the matrix element associated with the dominant channel $3p^6\ ^1S_0 \rightarrow 3p^5\epsilon d\ ^1P_1$ to go to zero resulting in the minimum at $h\nu \sim 50$ eV before changing sign to produce the secondary maximum at $h\nu \sim 80$ eV; at higher energies cancellation again reduces the overlap integral.

The theoretical predictions of McGuire (1968) and Amusya *et al* (1971) are illustrated by figure 5 where it is seen that general agreement between theory and experiment is

Table 3. Argon photoionization coefficients

Photon energy (eV)	k (total) (cm^{-1})
63·1	33·9
66·8	35·7
70·7	37·2
74·9	37·5
79·3	38·6
84·3	37·9
95·5	35·6
101·7	33·9
108·6	32·3
116·3	29·7
124·5	28·2
128·0	27·2
133·5	25·2
143·5	23·2
154·9	19·8
166·9	17·9
172·5	16·8
180·8	15·7
196·2	14·0
217·2	11·9

Error: ±3%

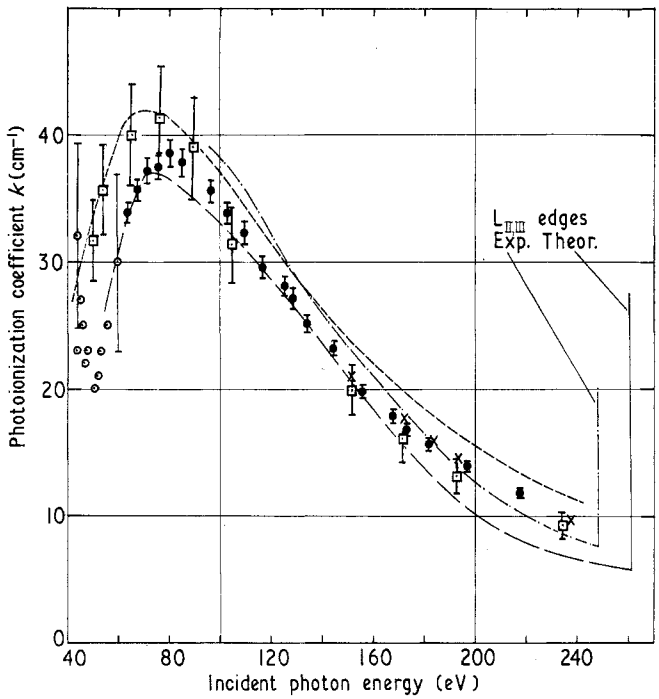

Figure 5. Photoionization coefficient of argon in the 40–250 eV photon energy range. Theory: – – – McGuire (1968); —— Amusya *et al* (1971). Experiment: ⊡ Lukirskii and Zimkina (1963); ⊙ Samson (1964c); –·–·– Haensel *et al* (1970) (±7% uncertainty); × Denne (1970); ● Present data.

good with the random phase approximation giving an excellent fit to the present results for photon energies in the 60–150 eV range but being up to 30% low for higher energies. The simpler unrelaxed core model predictions are up to 20% too high relative to the present data although giving better agreement with the less accurate experimental determinations of Lukirskii and Zimkina (1963) and Haensel *et al* (1970). However, the more sophisticated random phase approximation is preferred in this region since it predicts the spectral behaviour of the photoionization coefficient nearer threshold much more accurately than does the unrelaxed core model.

4. Conclusions

The present results consolidate the experimental data available for the spectral behaviour of the photoionization coefficients of helium, neon and argon resulting in, at worst, a ±5% accurate measure of these coefficients from threshold to $h\nu = 500$ eV. Any significantly larger percentage disagreement between theory and experiment must reflect on the adequacy of the theoretical models used.

Acknowledgments

The author would like to express his gratitude to Dr W McFarlane, Dr D T Stewart and

Mr J Lang for their advice and encouragement and also to the synchrotron staff for their cooperation during the experimental run. He would also like to thank the Science Research Council for financial support and the United Kingdom Atomic Energy Authority for the loan of the grazing incidence spectrometer.

References

Amusya M Ya, Cherepkov N A and Chernysheva L V 1971 *Sov. Phys.-JETP* **33** 90–6
Bell K L and Kingston A E 1967 *Proc. Phys. Soc.* **90** 31–7
—— 1970 *J. Phys.* B: *Atom. molec. Phys.* **3** 1433–6
Brown R L 1970 *Phys. Rev.* **1** 341–7
Byron F W and Joachain C J 1967 *Phys. Rev.* **164** 1–9
Carlson T A 1967 *Phys. Rev.* **156** 142–9
Denne D R 1970 *J. Phys.* D: *Appl. Phys.* **3** 1392–8
Dershem E and Schein M 1931 *Phys. Rev.* **37** 1238–45
Godwin R P 1969 *Springer Tracts in Modern Physics, Vol.* 51 (Berlin: Springer-Verlag)
Haensel R and Kunz C 1967 *Z. Angew, Phys.* **23** 276–95
Haensel R *et al* 1970 *DESY Report* 70/47
Henke B L, White R and Lundberg B 1957 *J. appl. Phys.* **28** 98–105
Lang J 1969 *ARU Report* (ARU-R1)
—— 1970 *Comp. Phys. Comm.* **1** 440–4
Lowry J F, Tomboulian D H and Ederer D L 1965 *Phys. Rev.* **137** A1054–7
Lukirskii A P and Zimkina T M 1963 *Bull. Acad. Sci. USSR, Phys. Ser.* **27** 808–11
Lukirskii A P, Brytov I A and Zimkina T M 1964 *Opt. Spectrosc.* **17** 234–7
Matsunaga F M, Jackson R S and Watanabe K 1965 *J. Quant. Spectrosc. Radiat. Transfer* **5** 329–33
McGuire E J 1968 *Phys. Rev.* **175** 20–30
Samson J A R 1964a *J. Opt. Soc. Am.* **54** 6–15
—— 1964b *J. Opt. Soc. Am.* **54** 876–8
—— 1964c *J. Opt. Soc. Am.* **54** 420–1
—— 1965 *J. Opt. Soc. Am.* **55** 935–7
Samson J A R 1969 *Phys. Rev. Lett.* **22** 693–4
Sewell K G 1965 *Phys. Rev.* **138** A418–21
Sokolov A A and Ternov I M 1968 *Synchrotron Radiation* (Oxford: Pergamon Press)
Stewart A L and Webb T G 1963 *Proc. Phys. Soc.* **82** 532–6
Watson W S and Morgan F J 1969 *J. Phys.* B: *Atom. molec. Phys.* **2** 277–82
Wheeler J A 1933 *Phys. Rev.* **43** 258–63